Analysis of the slope efficiency for terahertz quantum-cascade lasers

L. Schrottke,[a] M. Wienold, M. Giehler, R. Hey, and H. T. Grahn
Paul-Drude-Institut für Festkörperelektronik, Hausvogteiplatz 5-7, 10117 Berlin, Germany

(Received 4 August 2010; accepted 4 October 2010; published online 18 November 2010)

The slope efficiency is, in addition to the threshold current density and operating voltage, a decisive target value for the operation of quantum-cascade lasers (QCLs) in order to achieve an optimal total efficiency for the conversion of electrical input power into optical output power. We analyze the light-current characteristics for a set of similar, high-power, *bound-to-continuum* terahertz QCLs. The calculated internal slope efficiency shows a clear dependence on the height and thickness of the barriers. In contrast to the simulations, we found experimentally a significant difference in the threshold current densities and slope efficiencies for QCLs with nominally identical layer structures, which we mainly attribute to different line broadening. © *2010 American Institute of Physics*. [doi:10.1063/1.3511470]

I. INTRODUCTION

Quantum-cascade lasers (QCLs) for the terahertz (THz) spectral region are promising light sources for a variety of applications such as THz imaging as well as absorption spectroscopy and are used as local oscillators in heterodyne receivers.[1] To date, however, cooling of THz QCLs is still necessary as so far the maximum operating temperature of THz QCLs is well below 200 K. The operation of THz QCLs with a large wall plug efficiency in continuous-wave mode using coolant-free mechanical coolers[2] provides an acceptable alternative to the search for lasers with substantially increased maximum operating temperatures.

Meanwhile, the basic principles for the design of QCLs such as an efficient extraction of carriers out of the lower laser state as well as the suppression of leakage out of the upper laser state have been well established, in particular for the mid-infrared spectral region, and fundamental limitations have been discussed.[3] However, the role of the carrier redistribution due to stimulated emission, which is controlled by the gain clamping due to the gain-equals-loss condition, deserves particular attention in the design of QCL structures. Recent simulations have shown that this redistribution may lead to a spectral shift in the gain maximum and to an enhancement or even appearance of negative differential conductivity.[4] Therefore, the inclusion of stimulated emission into the simulation is expected to optimize the design procedure insofar as the internal slope efficiency can be treated as an additional target value. The combination of a low threshold current density with a low operating voltage together with a large slope efficiency are crucial for a large wall plug efficiency.

In this paper, we present a model for the calculation of the slope efficiency with acceptable numerical effort and compare the calculated values with experimental data for four THz QCLs with different barrier heights and thicknesses. The potential for design improvements is discussed.

The gain in QCLs is provided by population inversion between subbands due to resonant tunneling. For the description of carrier transport and the prediction of intersubband gain, theoretical models based on nonequilibrium Green functions,[5–7] microscopic theories using Monte Carlo simulations,[8,9] and the combination of a one-dimensional system of rate equations with the three-dimensional calculation of intersubband scattering times[10] are well established. Although in principle possible for all approaches, the photon-electron coupling has so far mainly been included in a few Monte Carlo simulations[11,12] rather than in the comprehensive quantum theory, mainly due to the enormous numerical effort necessary for simulations of THz QCLs. Recently, Terazzi and Faist[13] have included the optical field in the transport equations for a density matrix approach for mid-infrared QCLs.

While Jirauschek[12] discusses the maximum output power for a *resonant-longitudinal-optical-phonon design* with four quantum wells in each period in the framework of Monte Carlo simulations, Faist[3] gives a general expression for the slope efficiency derived for a three-level system. In particular in the case of THz QCLs based on *bound-to-continuum* designs, which rely on a delicate balance between various intersubband transitions, quantitative results for the slope efficiency are rather ambitious for Monte Carlo simulations and, eminently, for the treatment of nonequilibrium Green functions due to the numerical challenges. Therefore, an efficient design tool relies preferably on a momentum-independent scattering-rate model.

II. MODEL

We include stimulated emission into a scattering-rate model with total intersubband scattering rates approximated by $T_{ij}=\tau(\Delta E)|D_{ij}|^2$. The factorization of the scattering rates into the dipole matrix element D_{ij} and a function $\tau(\Delta E)$ of the transition energies $\Delta E=E_i-E_j=E_{ij}$ is used to simulate intersubband transitions due to electron-phonon scattering, electron scattering at impurities, and even due to electron-electron scattering, since the form factor for the scattering events can be approximated to be proportional to D_{ij}, in particular for electron-phonon scattering. Although the factorization cannot take into account the real nature of the scat-

[a]Electronic mail: lutz@pdi-berlin.de.

tering processes, it allows to relate them to the envelope functions and subsume them into a single term depending just on the transition energy. This approach allows to approximately evaluate the gain, operating voltage, and typical current densities with a reasonable numerical effort.[14] In this framework and following Refs. 4 and 15, stimulated photon emission and absorption is included as an additional scattering event for the electrons so that the scattering rates are now defined by

$$T_{ij} = |D_{ij}|^2 \left[\tau(\Delta E) + \frac{\pi e^2}{c n_B \varepsilon_0} \sum_k \omega_k \Gamma(\omega_k) \Phi_k L_{ij}(\omega_k) \right], \quad (1)$$

with $n_B=3.61$ for the background refractive index at THz frequencies and $\Gamma(\omega_k)$ denoting the optical confinement factor as well as $\nu_k=\omega_k/(2\pi)$ the photon frequency for the cavity mode k. e denotes the elementary charge, c the vacuum speed of light, and ε_0 the vacuum permittivity. The transition rates depend on the photon flux Φ_k (in units of per centimeter square per second) in the respective mode interacting with the intersubband transition. The Lorentzian line shape L_{ij} is given by

$$L_{ij}(\omega) = \frac{\gamma_b/2\pi}{(\hbar\omega - E_{ij})^2 + (\gamma_b/2)^2}, \quad (2)$$

with a broadening parameter $\gamma_b=\gamma_i+\gamma_j+2\gamma_0$, which is determined by the lifetime broadening γ_i and γ_j of the states $\langle i|$ and $\langle j|$ and an additional broadening parameter γ_0 due to for example interface roughness scattering.[7,16] We use the broadening parameter γ_0 in order to simulate inhomogeneous broadening in a simplified way. $\hbar$ denotes Planck's constant. The iteration for the self-consistent solution of the Schrödinger and Poisson equations using the system of scattering-rate equations will now include the laser rate equations. During the iteration, Φ_k will be increased (decreased) when the gain

$$g(\omega) = \frac{\omega\pi e^2}{c n_B \varepsilon_0 l_p} \sum_{i,j}^{(E_i>E_j)} (N_i - N_j)|D_{ij}|^2 L_{ij}(\omega), \quad (3)$$

is larger (smaller) than the optical losses α, i.e.,

$$\frac{d\Phi_k}{dt} \sim [\Gamma(\omega_k) g(\omega_k) - \alpha][\Phi_{k,0} + \Phi_k], \quad (4)$$

with l_p denoting the period length and $\Phi_{k,0}$ the flux due to spontaneous emission ($\Phi_{k,0}=0$ for absorption). In order to obtain solutions of the form $\Phi_k(E_k)\neq 0$, spontaneous emission has to be included. Finally, the iteration procedure arrives at the steady state with $d\Phi_k/dt=0$ for all modes and a significant value $\Phi_{k,\mathrm{las}}\neq 0$ for the lasing mode. The steady state corresponds to the gain-equals-loss condition $g=\alpha/\Gamma(\omega_{k,\mathrm{las}})=\tilde{\alpha}$.

We identify the total emission ($\Delta E>0$) and absorption ($\Delta E<0$) rates for photons per period and per unit area of the laser in the steady state $g=\tilde{\alpha}$ from the above equations by

$$T_{ij}^{\mathrm{phot}} = |D_{ij}|^2 \frac{\pi e^2}{c n_B \varepsilon_0} \sum_k \omega_k \Gamma(\omega_k) \Phi_k(\omega_k) L_{ij}(\omega_k). \quad (5)$$

The power emitted or absorbed per period by the transition $\langle i| \rightarrow \langle j|$ inside the cavity is

$$P_{ij} = \pm N_i T_{ij}^{\mathrm{phot}} h\nu_{\mathrm{phot}} A_{\mathrm{bar}}, \quad (6)$$

with N_i denoting the carrier sheet density for state $\langle i|$, $h\nu_{\mathrm{phot}}$ the photon energy of the lasing mode, and A_{bar} the area of the laser bar. The plus (minus) sign corresponds to an emission (absorption) process. The total power is obtained by summing the emitted and absorbed powers of all individual transitions $P_0=\Sigma_{ij}P_{ij}$ so that reabsorption due to intersubband transitions is taken into account. Note that, in steady state, only the product $\Gamma(\omega_k)\Phi_k(\omega_k)$ can be determined, not the individual factors, and the value of P_0 depends on the ratio $\alpha/\Gamma(\omega_{k,\mathrm{las}})$. For the numerical investigations, $\tilde{\alpha}=\alpha/\Gamma(\omega_{k,\mathrm{las}})$ and γ_0 are free parameters, which depend mainly on the specific laser cavity and the structural perfection, respectively, rather than on the layer structure.

The internal slope efficiency per period $S_{\mathrm{int}}=dP_0/dI=\eta\hbar\omega/e$ with $I=jA_{\mathrm{bar}}$ is related to the differential efficiency η, which is a measure of the average number of photons emitted by each additional electron passing through one period of the cascade. The maximum theoretical value $S_{\mathrm{int}}^{\mathrm{max}}=\hbar\omega/e$ corresponds to one photon per electron, if we neglect nonlinear effects such as two-photon emission. In the case of for instance two-photon emission, the sum of both photon energies $\hbar(\omega_1+\omega_2)$ has to be considered, which, however, corresponds to the transition energy in the same way as $\hbar\omega$ does in the linear case. If several transitions would contribute to the lasing emission, in a serial way within one period, $S_{\mathrm{int}}^{\mathrm{max}}$ would scale with their number. Such possible multiple emission processes are taken into consideration by our model but do usually not occur. The difference between this maximum value and a value of S_{int} calculated for a particular design is a measure for additional nonradiative transitions above threshold. For a three-level model, it can be approximated according to Eq. (3) of Ref. 3 by the ratio of the lower-state lifetime and the scattering time for the transition between the upper and lower states. In our multi-level model, also increasing currents through parasitic states can affect the calculated internal slope efficiency.

In order to compare the numerical results with experimental data, the power P_f emitted through one facet as well as the external slope efficiency $S=dP_f/dI$ have to be determined. The power P_0N_{per} emitted by N_{per} periods into the resonator has to be split into the power P_a absorbed in the waveguide and the power $2P_f$ extracted out of the cavity through the two facets. P_a is significantly affected by the waveguide losses α_w, which are mainly caused by free-carrier absorption. The net optical output can be written as

$$P_f = \frac{P_0}{2} \frac{N_{\mathrm{per}}}{\alpha_w L} \frac{(1-R)(1-e^{-\alpha_w L})}{1-Re^{-\alpha_w L}}, \quad (7)$$

with L denoting the length of the laser bar and R the reflection coefficient for a single facet. Equation (7) is derived assuming multiple reflections of the light ray with exponen-

tially decaying intensity inside the resonator. This picture yields an intensity distribution of the form $1-A\cosh(\alpha_w x)$ with the position $x=0$ in the center of the resonator and $x=\pm L/2$ at the facets. The constant A becomes larger for increasing mirror losses and decreasing waveguide losses and/or resonator lengths. Using for example $R=0.3$ and $\alpha_w L=1$, the intensity is reduced by about 12% at the facets compared to the maximum in the center of the resonator. Introducing mirror losses in the form $L\alpha_m=-\ln R$, the net power for small losses can be approximated by

$$P_f \approx \frac{P_0}{2} N_{\mathrm{per}} \frac{\alpha_m}{\alpha}, \tag{8}$$

with $\alpha=\alpha_w+\alpha_m$ as used in Eq. (4) for the optical losses. This approximation corresponds to Eq. (2) of Ref. 3 and to a position-independent photon flux. While Eq. (8) is often a good approximation for Eq. (7), in some cases it does not appear to be appropriate for an analysis of the slope efficiencies. For example, the calculated length dependence of the slope efficiency according to Eq. (7) using $R=0.3$ and $\alpha_w=10\ \mathrm{cm}^{-1}$ can be approximated by Eq. (8) when $\alpha_w=20\ \mathrm{cm}^{-1}$, i.e., a value as twice as large, is used. In our notation, gain and losses are related to intensities rather than amplitudes.

III. SAMPLES

We compare simulated data and measured slope efficiencies for four rather similar THz QCLs. Structures A1 and A2 consist of $\mathrm{GaAs}/\mathrm{Al}_{0.15}\mathrm{Ga}_{0.85}\mathrm{As}$ heterostructures, which are based on a *bound-to-continuum* transition. For efficient injection, a transition which is resonant to the longitudinal optical phonon is used. The details of the design have been presented elsewhere.[17,18] The samples A1 and A2 have nominally identical layer thicknesses but their periods as determined by x-ray analysis differ from their design values by −1% and +6%, respectively. For samples B and C, $\mathrm{Al}_{0.25}\mathrm{Ga}_{0.75}\mathrm{As}$ barriers are used in order to reduce the effect of parasitic states on the current density. While the barrier and well thicknesses for sample B are identical to the nominal parameters for samples A1 and A2, the barrier thicknesses of sample C are reduced by a factor of 0.77 in order to obtain a similar coupling as in sample A and the well thicknesses remain the same. The reduced coupling in sample B is expected to result in a lower threshold current density and a lower output power. More important for our purpose, the weaker coupling is also expected to lead to a reduction in parasitic currents so that the slope efficiency may increase. The band structure and wave functions for sample B are shown in Fig. 1.

The samples, which consist of a 700 nm thick GaAs layer Si-doped with $2\times10^{18}\ \mathrm{cm}^{-3}$ on the substrate side, a 10 μm thick active region, and a 80 nm thick GaAs layer Si-doped with $5\times10^{18}\ \mathrm{cm}^{-3}$ on the top side, were grown by molecular-beam epitaxy on semi-insulating GaAs(100) substrates. The actual values of the layer thicknesses and the doping density for the cascade structure used in the simulations were obtained from an x-ray diffraction analysis of the (002) curves and capacitance-voltage measurements, respectively. While the doping density of samples A1 and B was determined to be $5\times10^{16}\ \mathrm{cm}^{-3}$, we found a value of $6\times10^{16}\ \mathrm{cm}^{-3}$ for samples A2 and C.

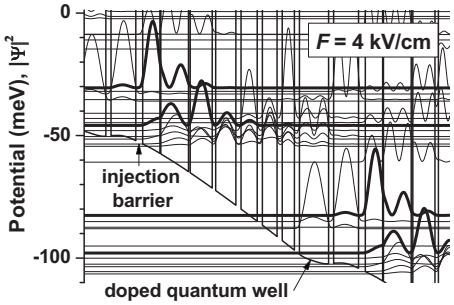

FIG. 1. Conduction band structure and squared moduli of the wave functions for sample B at an average field strength of 4 kV/cm. The layer sequence given in nm and starting from the injection barrier is **4.0**, 10.1, **0.5**, 16.2, **1.0**, 12.9, **2.0**, 11.8, **3.0**, 9.5, **3.0**, 8.6, **3.0**, 7.1, **3.0**, 17.0, **3.0**, 14.5. Bold symbols indicate the $\mathrm{Al}_{0.25}\mathrm{Ga}_{0.75}\mathrm{As}$ barriers. The underlined quantum well is Si-doped with a concentration of $5\times10^{16}\ \mathrm{cm}^{-3}$.

The wafers were processed for single-plasmon waveguides with a typical size of the laser stripes of $0.2\times3.4\ \mathrm{mm}^2$. The laser emission was studied in pulsed-mode operation with current pulses of 500 ns and a repetition rate of 5 kHz at temperatures of the sample holder between 10 and 15 K. For these measurements, the current density was varied from just above the threshold current density j_{th} to the maximum operating current density. The infrared spectra were recorded using a Fourier-transform spectrometer with a spectral resolution of $0.12\ \mathrm{cm}^{-1}$. Measurements of the output power were performed with a pyroelectric powermeter in front of the cryostat window. We used a light pipe attached to the powermeter and a cone in front of the laser to maximize the collection efficiency, which is assumed in the following to be unity. For sample B, additional lasers have been fabricated with 0.1 mm wide laser bars and lengths of 0.76, 1.0, as well as 3.4 mm and a laser with a size of $0.2\times1\ \mathrm{mm}^2$.

IV. NUMERICAL RESULTS

We calculated the gain spectra and the current density j as a function of the electric field strength F with the inclusion of stimulated emission. The line broadening is determined by the total lifetime of the states and a value for γ_0 of 0.5 meV, which leads to a linewidth of the gain spectra similar to the observed width of the envelope of the lasing spectra. The simulations were carried out for three values of the optical losses $\tilde{\alpha}=20\ \mathrm{cm}^{-1}$, $30\ \mathrm{cm}^{-1}$, and $40\ \mathrm{cm}^{-1}$, which correspond to $\alpha=9\ \mathrm{cm}^{-1}$, $13.5\ \mathrm{cm}^{-1}$, and $18\ \mathrm{cm}^{-1}$, respectively, assuming an optical confinement factor of $\Gamma(\omega_k)=0.45$. For a more detailed discussion of these values, see Sec. V. To investigate the influence of the broadening parameter, we also simulated the internal slope efficiency for $\tilde{\alpha}=20\ \mathrm{cm}^{-1}$ and $\gamma_0=1.0$ meV.

Figures 2(a) and 2(b) show, as an example, the gain spectra and the $j-F$ characteristics, respectively, for sample B using an optical loss of $\tilde{\alpha}=30\ \mathrm{cm}^{-1}$ and $\gamma_0=0.5$ meV. The arrows in Fig. 2(a) indicate the observed range of lasing

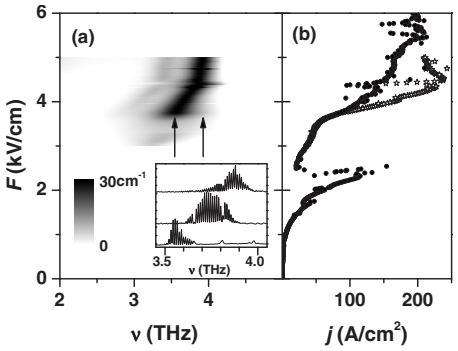

FIG. 2. (a) Calculated gain spectra for sample B in a gray-scale representation as a function of frequency ν and electric field strength F. White areas correspond to no gain or losses, black areas correspond to a gain value of 30 cm^{-1}. The arrows indicate the range of observed lasing frequencies. The inset shows three typical laser spectra at threshold (70 A/cm^2), at intermediate currents (180 A/cm^2), and at maximum output power (240 A/cm^2) from bottom to top. (b) Calculated current density j for sample B with (open symbols) and without inclusion of stimulated emission (full symbols).

frequencies, which are close to the calculated gain maximum. The inset in Fig. 2(a) shows typical lasing spectra for this sample.

The calculated internal slope efficiencies for one period can be determined from the optical output-current density characteristics shown in Fig. 3 for sample B. Note that the optical output power per laser bar is defined as $p_{bar}=P_0/A_{bar}$. Figure 3(a) illustrates the dependence of the threshold current density and the internal slope efficiency on $\tilde{\alpha}$ for $\gamma_0=0.5$ meV. An increase in $\tilde{\alpha}$ from 20 to 40 cm^{-1} leads to a decreasing output power and increasing values for j_{th} from about 70 to about 100 A/cm^2, which agree approximately with the well established relation $j_{th}\sim\alpha$. However,

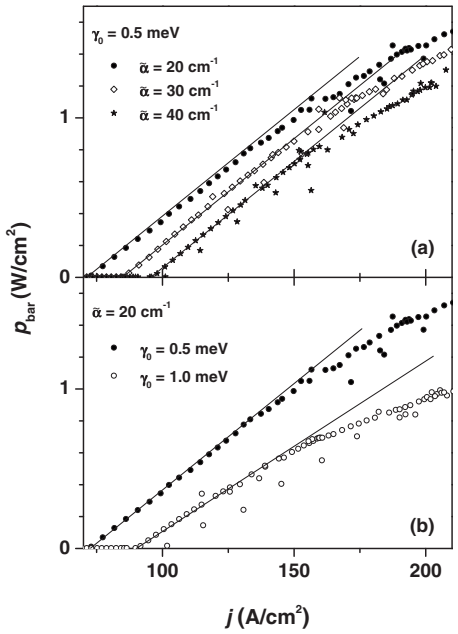

FIG. 3. Calculated internal output power per period $p_{bar}=P_0/A_{bar}$ as a function of current density for sample B (a) for three values of $\tilde{\alpha}$ and $\gamma_0=0.5$ meV as well as (b) for $\tilde{\alpha}=20$ cm^{-1} and two values of the broadening parameter γ_0. The thin solid lines correspond to the slope efficiencies just above threshold.

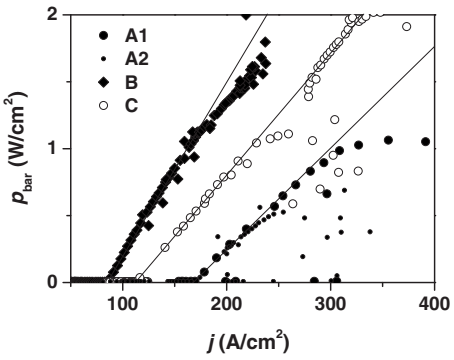

FIG. 4. Calculated internal output power per period p_{bar} as a function of current density for samples A1, A2, B, and C using $\tilde{\alpha}=30$ cm^{-1} and $\gamma_0=0.5$ meV. The thin solid lines correspond to the slope efficiencies just above threshold.

the internal slope efficiency remains almost constant at about 13 mW/A per period so that it appears to be determined mainly by the subband structure.

The effect of changing the value for γ_0 from 0.5 to 1.0 meV on the calculated $p_{bar}-j$ characteristics is, however, more significant as demonstrated in Fig. 3(b) for $\tilde{\alpha}=20$ cm^{-1}. In this case, not only the threshold current density is shifted from 70 to 90 A/cm^2 but also the slope efficiency is reduced from 13 mW/A to about 10 mW/A per period. Furthermore, even the shape of the $p_{bar}-j$ characteristic is changed, which clearly demonstrates that the balance of intersubband transitions and, hence, the charge distribution are affected by stimulated emission as well as absorption processes. In particular, an increase in the broadening parameter γ_0 can lead to a stronger influence of the absorption lines in the vicinity of the gain maximum as their widths are also increased. Insofar as inhomogeneous broadening is caused by interface roughness, this mechanism acts in addition to elastic scattering of electrons at the interfaces, which, however, cannot be included in a momentum-independent model.

Figure 4 shows the calculated $p_{bar}-j$ characteristics for all four samples (using $\tilde{\alpha}=30$ cm^{-1} and $\gamma_0=0.5$ meV). From the slope just above threshold (see thin solid lines), we obtain values of 7, 13, and 9 mW/A per period for samples A1, B, and C, respectively. The sample with the weakest coupling (B) exhibits the largest value, which is close to the theoretical limit S_{int}^{max} of 15.7 mW/A for 3.8 THz. The calculated slope efficiencies for samples A1 and A2 are almost identical at threshold. At the same time, the larger period length of sample A2 leads to a redshift in the gain maximum from about 3.4 THz for sample A1 to about 3.0 THz for sample A2. The calculated gain maxima agree well with the observed range of lasing frequencies from 3.3 to 3.55 THz for A1 and from 2.7 to 3.3 THz for A2.

V. EXPERIMENTAL RESULTS

For the comparison of the simulated slope efficiencies with experimental data, the net output power according to Eq. (7) has been determined. For the reflection coefficient R, we use the value 0.3, while the number of periods is 85. A decisive parameter for the comparison of the output power P_f and the total power P_0 is the value of α_w for the wave-

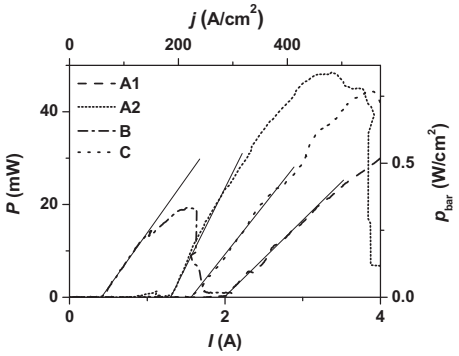

FIG. 5. Measured output power P as a function of current I for samples A1, A2, B, and C. The quantities j and p_{bar} have been converted from I and P using the nominal values of the area of the laser stripe and the waveguide losses according Eq. (7). The thin solid lines correspond to the slope efficiencies just above threshold.

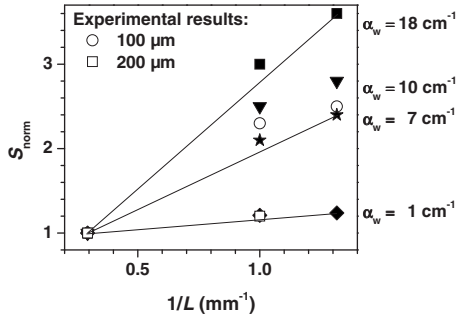

FIG. 6. Calculated relative slope efficiencies (solid symbols) using Eq. (7) with several values for α_w and for L=3.4, 1.0, and 0.76 mm divided by the value for L=3.4 as well as experimentally observed relative slope efficiencies (open symbols) for sample B (0.1 and 0.2 mm wide lasers). The thin solid lines show the exact $1/L$ behavior as a guide to the eye.

guide losses. Its value is estimated by both a numerical simulation of the waveguide properties and an experimental determination using the $1/L$-dependence of j_{th}. We estimate the waveguide losses for 0.2 and 0.1 mm wide lasers to be about α_w=10 cm^{-1} and α_w=18 cm^{-1}, respectively. The waveguide losses for the broader stripes are in agreement with a one-dimensional waveguide simulation using similar parameters as Ref. 19, yielding a value of 8 cm^{-1} due to free-carrier absorption. For the narrow laser stripes, additional losses due to for example light scattering at the sidewalls[20] are expected to become more significant and lead to the larger value for α_w.

For 3.4 mm long resonators, assuming α_m=3.5 cm^{-1} and α_w=10 cm^{-1}, we obtain for the net waveguide losses α=13.5 cm^{-1}, which has also been used for the numerical simulation of the slope efficiencies in Sec. IV. In particular for sample B, we find a very good quantitative agreement between the observed and calculated values for the threshold current density (about 70 A/cm^2) as well as the current density at maximum output (about 240 A/cm^2), which corresponds to the onset of negative differential conductivity in the simulated $j-F$ characteristics. Note that for this sample also the calculated gain spectra for this current range agrees rather well with the observed lasing frequencies. For the other three samples, the observed current densities are larger than the calculated ones.

The calculated slope efficiencies shown in Fig. 4 agree qualitatively with the experimental values depicted in Fig. 5 insofar as sample A1 exhibits the lowest slope efficiency, while sample B exhibits the largest one, if sample A2 is not taken into consideration. Similarly, A1 (B) has the largest (smallest) threshold current density for both the calculated and the observed values. For a quantitative comparison, we apply Eq. (7) using L=3.4 mm, R=0.3, and α_w=10 cm^{-1} and obtain P_f=8.5P_0 so that the net slope efficiencies of samples A1 (and A2), B, and C are expected to be 60 mW/A, 110 mW/A, and 77 mW/A respectively. However, the actual values as derived from the experimental output-current characteristics shown in Fig. 5 are 15 mW/A, 34 mW/A, 24 mW/A, and 23 mW/A for samples A1, A2, B, and C, respectively. Sample A2 exhibits the largest slope efficiency with a value of about one half of the calculated one. For the other three samples, the measured slope efficiencies amount to only 25%–30% of the calculated values.

The significant deviation of the measured values from the calculated ones may be attributed to an overestimation of the collection efficiency and/or to underestimated values for α and γ_0, although the simulations for sample B exhibit a good agreement with the experimental current densities at threshold and maximum output power. If we would assume for example α_w=18 cm^{-1}, which leads to P_f=4.9P_0 for the 3.4 mm long lasers, we would obtain a calculated slope efficiency of about 34 mW/A for sample A2 in good agreement with the observations.

For single-plasmon waveguides, the optical confinement is rather small so that a considerable portion of the modes reaches into the substrate. Light scattering at the backside of the substrate and/or at sidewalls of the laser stripes may affect the beam shape and hence the collection efficiency. In order to obtain additional information about the waveguide properties, we calculated the slope efficiency S as a function of $1/L$ according to Eq. (7). Figure 6 shows the calculated relative values S_{norm} (full symbols) versus $1/L$ for α_w=1, 7, 10, and 18 cm^{-1}. The experimental values for lasers with a width of 0.1 mm and lengths of 3.4, 1.0, and 0.76 mm as well as for lasers with a width of 0.2 mm and lengths of 3.4 and 1.0 mm are shown by open symbols. The experimentally observed $1/L$ behavior corresponds to values for α_w of about 8 and 1 cm^{-1}, which are significantly smaller than the experimentally determined values of 18 and 10 cm^{-1}. Starting from the assumption that laser light is scattered out of the waveguide modes into substrate modes, we may explain the observed $1/L$ behavior of S by a superposition of waveguide modes with substrate modes. We believe that substrate modes are not properly described by Eq. (7) because they may be affected by both, scattering at the rather rough substrate backside and multiple reflections at the side facets of the substrate. At the same time, the intrinsic absorption of the substrate modes is smaller, since the substrate is undoped. A scattering of light out of the detection direction may lead to a smaller measured output power as well as to a different length dependence of the slope efficiencies.

VI. DISCUSSION

In addition to some difficulties in the understanding of the impact of α on both the value and the $1/L$ dependence of S, the transport properties and the inhomogeneous broadening require some further discussion. As shown in Fig. 2(b), the interaction of the electron transport with stimulated emission can affect the onset and strength of negative differential conductivity. In particular for sample B, the calculated onset of negative differential conductivity induced by stimulated emission at about 4.5 kV/cm and 250 $\mathrm{A/cm^2}$ agrees with the measured current density at maximum output. We conclude that the interplay of stimulated emission with the electron transport in THz QCLs has to be taken into account when current instabilities are investigated. Furthermore, the systematic observation of larger current densities for the samples with lower barriers (A1 and A2) and thinner barriers (C) as expected from the model may be an indication of the limitations of our model as leakage currents for example due to scattering into quasicontinuum states[21] and effects due to the coherence of the subband states and their dephasing[22] are not included. However, the different values for j_{th} and S of the two very similar samples A1 and A2 show that fluctuations during the complete fabrication process may have an effect on these quantities of the same order of magnitude.

The inhomogeneous broadening γ_0 of the gain spectrum is affected, for instance, by interface roughness, which may be controlled to some extent by the growth conditions. A more comprehensive analysis of the structural perfection in terms of the average interface roughness inside the QCL structure would be necessary in order to determine the effect of structural perfection on the operating parameters, which is beyond the scope of this paper. In addition, an effect of inhomogeneities of the electric field distribution on γ_0 due to a spatially inhomogeneous Stark shift in the gain maximum cannot be excluded. The appearance of negative differential conductivity may even enhance these inhomogeneities. The simulations as shown in Fig. 3 clearly demonstrate an impact of γ_0 on the threshold current densities and slope efficiencies. Therefore, systematic numerical and experimental studies of the output characteristics of THz QCLs are expected to provide indirect but nevertheless valuable, information about processes, which lead to inhomogeneous broadening.

VII. CONCLUSIONS

We have shown that the slope efficiency for THz QCLs is important for comparing the simulated with the experimental results, in particular, as the resonator properties and inhomogeneous broadening of the gain spectra have a significant effect on the slope efficiency. While the calculated threshold current density rather than the internal slope efficiency is determined by the optical losses, the calculated external as well as the measured slope efficiencies are affected by the optical losses and the resonator length. The simulations have also shown that the internal slope efficiency depends on the inhomogeneous line broadening of the gain spectra. Finally, the calculated internal quantum efficiency is a measure for parasitic currents which may be reduced by increasing the barrier height. Therefore, the slope efficiency is also a meaningful target parameter for the design strategy of THz QCLs provided that the numerical tool allows to carry out the simulations with acceptable effort.

ACKNOWLEDGMENTS

The authors would like to thank W. Anders, K. Biermann, and M. Höricke for sample growth and processing.

[1] B. S. Williams, Nat. Photonics **1**, 517 (2007), and references therein.
[2] H. Richter, M. Greiner-Bär, S. G. Pavlov, A. D. Semenov, M. Wienold, L. Schrottke, M. Giehler, R. Hey, H. T. Grahn, and H.-W. Hübers, Opt. Express **18**, 10177 (2010).
[3] J. Faist, Appl. Phys. Lett. **90**, 253512 (2007).
[4] L. Schrottke, M. Giehler, M. Wienold, R. Hey, and H.T. Grahn, Physica E (Amsterdam) **42**, 2632 (2010).
[5] A. Wacker, Phys. Rev. B **66**, 085326 (2002).
[6] S.-C. Lee and A. Wacker, Phys. Rev. B **66**, 245314 (2002).
[7] T. Kubis, C. Yeh, P. Vogl, A. Benz, G. Fasching, and C. Deutsch, Phys. Rev. B **79**, 195323 (2009).
[8] R. C. Iotti and F. Rossi, Phys. Rev. Lett. **87**, 146603 (2001).
[9] C. Jirauschek, A. Matyas, and P. Lugli, J. Appl. Phys. **107**, 013104 (2010).
[10] K. Donovan, P. Harrison, and R. W. Kelsall, J. Appl. Phys. **89**, 3084 (2001).
[11] R. C. Iotti and F. Rossi, Rep. Prog. Phys. **68**, 2533 (2005).
[12] C. Jirauschek, Appl. Phys. Lett. **96**, 011103 (2010).
[13] R. Terazzi and J. Faist, New J. Phys. **12**, 033045 (2010).
[14] L. Schrottke, M. Giehler, M. Wienold, R. Hey, and H. T. Grahn, Semicond. Sci. Technol. **25**, 045025 (2010).
[15] N. Vukmirović, V. D. Jovanović, D. Indjin, Z. Ikonić, P. Harrison, and V. Milanović, J. Appl. Phys. **97**, 103106 (2005).
[16] C. Jirauschek and P. Lugli, J. Appl. Phys. **105**, 123102 (2009).
[17] M. Wienold, L. Schrottke, M. Giehler, R. Hey, W. Anders, and H. T. Grahn, Electron. Lett. **45**, 1030 (2009).
[18] M. Wienold, L. Schrottke, M. Giehler, R. Hey, W. Anders, and H. T. Grahn, Appl. Phys. Lett. **97**, 071113 (2010).
[19] S. Kohen, B. S. Williams, and Q. Hu, J. Appl. Phys. **97**, 053106 (2005).
[20] F. Toor, D. L. Sivco, H. E. Liu, and C. Gmachl, Appl. Phys. Lett. **93**, 031104 (2008).
[21] X. Gao, D. Botez, and I. Knezevic, J. Appl. Phys. **101**, 063101 (2007).
[22] H. Callebaut and Q. Hu, J. Appl. Phys. **98**, 104505 (2005).